Sub-barrier fusion of weakly bound ^{6}Li with ^{58}Ni

E. F. Aguilera,[*] E. Martinez-Quiroz, P. Amador-Valenzuela, D. Lizcano, and A. García-Flores
Departamento de Aceleradores, Instituto Nacional de Investigaciones Nucleares, Apartado Postal 18-1027, Código Postal 11801, México, Distrito Federal, Mexico

J. J. Kolata, A. Roberts,[†] G. V. Rogachev,[‡] and G. F. Peaslee
Physics Department, University of Notre Dame, Notre Dame, Indiana 46556-5670, USA

V. Guimarães
Instituto de Fisica, Universidade de São Paulo, Rua do Matão 1371, 05508-090 São Paulo, São Paulo, Brazil

F. D. Becchetti, A. Villano,[§] M. Ojaruega,[‖] Y. Chen,[¶] and H. Jiang[**]
Physics Department, University of Michigan, Ann Arbor, Michigan 48109-1040, USA

M. Febbraro
Physics Division, Oak Ridge National Laboratory, Oak Ridge, Tennessee 37830, USA

P. A. DeYoung
Department of Physics, Hope College, Holland, Michigan 49423-9000, USA

T. L. Belyaeva
Universidad Autónoma del Estado de México, Código Postal 50000, Toluca, Mexico
(Received 25 May 2017; published 23 August 2017)

Evaporation-proton yields were measured for the fusion of the weakly bound nucleus ^{6}Li on a ^{58}Ni target at six near- or sub-barrier bombarding energies. Effects of the one-neutron transfer reaction were estimated and corrections made. Total-fusion cross sections were deduced using calculated proton multiplicities. The resulting fusion excitation function shows a considerable enhancement with respect to calculations for a bare potential. Inelastic couplings are estimated to have insignificant effects on such fusion. The sum of total fusion plus one-neutron transfer cross sections nearly saturates the total reaction cross section in the energy region measured. Comparison with previous results appropriately scaled for the ^{6}Li + (^{59}Co, ^{64}Ni, ^{64}Zn) systems shows good consistency except for some data spread at the lower energies.

DOI: 10.1103/PhysRevC.96.024616

I. INTRODUCTION

The near- and sub-barrier fusion process for reactions induced by weakly bound projectiles, stable or radioactive, has been the subject of many recent studies, both experimental and theoretical. Several relevant updated reviews have been published in the last few years [1–3].

Of the stable, weakly bound nuclei, one of the most interesting is perhaps the ^{6}Li nucleus. Although stable, it has no bound excited states and a separation energy of only 1.47 MeV for splitting into ^{4}He and ^{2}H. Thus breakup and/or cluster transfer (CT) channels might be expected to be important in interactions with other nuclei. The need to take the breakup channel into account has been extensively discussed in relation to the ^{6}Li + ^{59}Co near-barrier fusion data of Ref. [4]. Continuum-discretized coupled-channel (CDCC) calculations performed for this system [5,6] have shown that breakup couplings significantly enhance the near- and sub-barrier total fusion cross sections, thus bringing the calculations into agreement with the data. This effect occurs despite the fact that the breakup contribution to the respective total reaction cross section is rather small, being actually about 2 orders of magnitude lower than the corresponding fusion part [6–8].

In a detailed study of quasielastic backscattering with a ^{64}Zn target at energies near the Coulomb barrier [9], it became clear that couplings with inelastic excitations of the target and/or projectile alone are not enough to explain the data. Subsequent CDCC analyses of the corresponding elastic scattering angular distributions for this system [10] showed

[*]eli.aguilera@inin.gob.mx
[†]Present address: Physics Department, University of South Dakota, Vermillion, SD 57069.
[‡]Present address: Department of Physics & Astronomy and Cyclotron Institute, Texas A&M University, College Station, Texas 77843.
[§]Present address: Physics Department, University of Minnesota, Minneapolis, MN 55455.
[‖]Present address: ICESS/Defense Threat Reduction Agency, 8725 John J. Kingman Road, Fort Belvoir, VA 22060.
[¶]Present address: 21st Century Oncology Inc., Suite 104, 555 D'onofrio Drive, Madison, WI 53719.
[**]Present address: Bruker AXS Inc., 5465 East Cheryl Parkway, Fitchburg, WI 53711.

important effects of coupling to breakup channels. At the lowest incident energies a significant effect of coupling to resonant states of ^{6}Li also was found.

Fusion studies for that system, where cross sections for the production of heavy residues resulting from the ^{6}Li + ^{64}Zn reaction were measured [11], indicate that the observed fusion enhancement at sub-barrier energies also cannot be explained by couplings between elastic and inelastic channels. Evidence was found by comparing with statistical model predictions that, while complete fusion (CF) dominates at energies well above the barrier, nucleon-transfer as well as incomplete fusion (ICF) with a deuteron (d) and/or d transfer might be affecting the sub-barrier yields. Both mechanisms (nucleon transfer and d transfer) would produce heavy residues indistinguishable from those produced by fusion and therefore they would be phenomenologically included in the reported total fusion (TF) yield.

Recent measurements for breakup of ^{6}Li on targets of ^{58}Ni and ^{64}Zn [12] showed that for an energy close to but below the barrier most of the breakup events occur far from the target, where absorption of the fragments is unlikely and so no effect on ICF is expected. Some authors have suggested that the charged fragment absorption leading to incomplete fusion is minimal at sub-barrier energies [12,13] and it is generally accepted that the ICF cross sections involving medium and light mass targets are much smaller than those corresponding to CF [14]. Because some energy must be used to separate the projectile clusters, the remaining energy of the fragments after breakup is usually lower with respect to the corresponding barrier than that of the original projectile, so ICF could hardly be expected to dominate at sub-barrier energies. In any case, yield contaminants from either deuteron or single-nucleon transfers do actually seem to be likely candidates to at least partially explain the large sub-barrier fusion cross sections reported for the ^{6}Li + ^{64}Zn data of Ref. [11]. CDCC calculations including couplings between elastic scattering, breakup, and fusion are needed to shed light on this issue. Nonetheless, the different data sets for fusion involving ^{6}Li projectiles are still far from being fully understood.

In the present work new fusion data for the system ^{6}Li + ^{58}Ni are reported to better elucidate this issue. Evaporation-proton yields were measured at six sub-barrier energies (except the highest energy, which was above but close to the barrier) and statistical model calculations were performed to deduce the respective fusion cross sections. Preliminary results were previously reported in Ref. [15], but only included results for three energies. In addition to data for several new energies, the present work presents a more thorough analysis using three different statistical model codes. It includes as well a discussion of possible effects of ICF and direct reactions.

The experimental procedure and results are described in Sec. II, where possible effects of some direct reactions also are discussed. In Sec. III, the data are compared with barrier-penetration-model calculations and with coupled-channel calculations where the most relevant inelastic channels are taken into account. Possible effects of incomplete fusion and direct cluster transfer are also discussed there. In Sec. IV, the results are compared with other fusion measurements for ^{6}Li projectiles and, finally, a summary and the conclusions deduced from the present work are presented in Sec. V.

II. EXPERIMENTAL DETAILS AND RESULTS

The present experiment is the final part of an extensive project in which a mixed secondary beam of ^{6}Li, ^{7}Be, and ^{8}B was generated at the TwinSol radioactive nuclear beam facility [16] at the University of Notre Dame (UND) and used to bombard several Ni targets. Beam bunching and pulse selection were applied to the primary beam and, for each beam component, the protons emitted by the corresponding fused system were measured at backward angles, identifying them by time of flight (TOF). A condensed description of the general experimental procedure is given in Ref. [17], where the results for the fusion of proton-halo ^{8}B + ^{58}Ni are reported. Additional details concerning the ^{7}Be + ^{58}Ni radioactive beam measurements are given in Ref. [18]. Specific details related to the ^{6}Li data are described here.

A primary ^{6}Li^{3+} high-intensity beam with energies between 31 and 38 MeV, delivered by the UND FN tandem accelerator, was used to bombard a 2.5-cm-long primary gas target of ^{3}He at a pressure of 1 atm. The ^{6}Li isotope in the secondary beam corresponds to quasielastic scattering of the primary beam and is therefore the most abundant component of the mixed secondary beam. Secondary beam rates (at target) of 0.6–4.0 × 10^{7} particles/s were typically produced. The respective energy resolution was 0.6–0.8 MeV [full width at half maximum (FWHM)], with a typical time spread of 7–10 ns (FWHM). The actual time resolution was about 2 ns, but the time-energy correlation produces this spread. (For only one run, the time spread was ∼15 ns). A sample beam spectrum is presented in Fig. 1, which shows that the ^{6}Li beam can be nicely separated by TOF from the other major components, but not from a satellite ^{4}He^{2+} beam. However, the intensity of the latter beam is quite weak compared to that of ^{6}Li and, in addition, corresponds to low-energy α particles unlikely to induce evaporation protons in reactions with ^{58}Ni. Taking the example of the mixed beam shown in Fig. 1, the estimated contribution of protons from ^{4}He + ^{58}Ni to the total proton

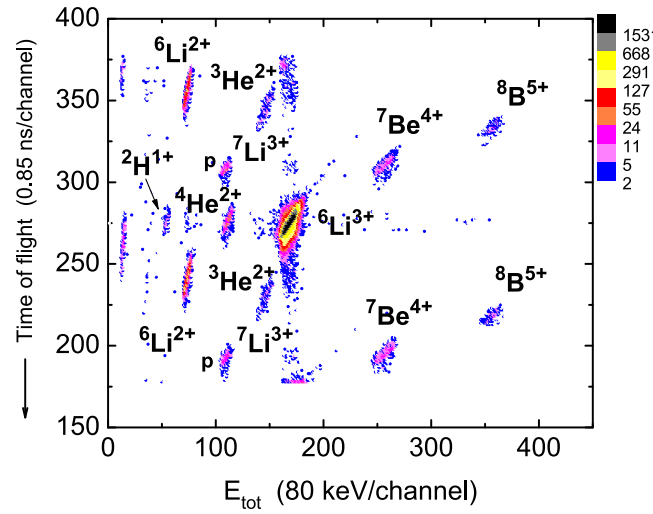

FIG. 1. Mixed secondary beam spectrum, obtained with a detector temporarily placed at the target position with the beam rate lowered by 3 orders of magnitude.

TABLE I. Targets and detectors used in the different stages of the ^{6}Li + ^{58}Ni experiment. E_{in} is the incident (lab) energy while $E_{c.m.}$ is its weighted mean throughout the target [with $\sigma_{fus}(E)$ as the weighting function], transformed to the center-of-momentum frame of reference.

Stage	Target thickness (mg/cm^2)	Target size (cm)	Backward telescopes (deg)	Monitors (deg)	E_{in} (MeV)	$E_{c.m.}$ (MeV)
1	1.36	2.5 (diameter)	120, 135, 150	45, 60[a]	13.2	11.7 ± 0.2
					14.4	12.7 ± 0.3
2	5.60	13 × 13	113, 128, 143, 158	±45[b]	10.8	9.1 ± 0.2
3	2.22	8.9 × 8.9	113, 128, 143, 158	±45[b]	11.5	9.9 ± 0.3
					12.7	11.0 ± 0.3
					13.7	11.9 ± 0.3

[a] E-ΔE telescopes.
[b] Single detectors.

yield is 0.4%. Therefore, a possible contamination of the data with protons induced by ^{4}He reactions can be safely neglected.

The experiment was performed in three stages, covering a total of six bombarding energies, as indicated in Table I. Natural Ni targets were used, with thicknesses and sizes as shown in Table I, with appropriate corrections applied to account for the presence of isotopes other than ^{58}Ni. As mentioned in Ref. [17], the validity of these corrections was verified with ^{8}B beam data by comparing with equivalent measurements using an enriched ^{58}Ni target.

Silicon surface-barrier detectors were used both for the backward telescopes and for the beam monitors. The thin (ΔE) detectors of the backward telescopes were 65–95 μm thick for stage 1, while they had a typical thickness of ∼40 μm for all other stages. The thickness of the monitor ΔE detectors used in stage 1 was ∼20 μm. The thick (E) detectors used as the monitors in stage 2 had a thickness of 150 μm, and they were ∼1000 μm thick for the other measurements. Solid angles were defined by collimators of 18–25 mm in diameter placed in front of all telescopes and monitors. The collimators were thick enough to stop all possible protons. The solid angles were ∼30–50 msr in stage 1 for the backward telescopes, and about 8.5 msr in stages 2 and 3. They were always set between 11 and 18 msr for the monitors.

Background determinations were performed by doing blank-target measurements under the same conditions as the measurements with the Ni target. The details of the corresponding procedure have been described in Ref. [18]. It was determined that the presence of background protons in the data was insignificant in the present case, with typical contributions around 1%.

Figure 2 shows the experimental results obtained for the proton angular distributions at back angles, along with statistical model calculations using the code PACE2 [19,20]. Default values were used for all input parameters in this code, except for the parameter "expsig," whose default value is 0. Instead, for each energy the fusion cross section (σ_{fus}) was used in expsig as a fitting parameter, which yields a corresponding curve for the proton angular distribution $d\sigma_p/d\Omega$. One may notice that the experimental points are consistent with model expectations, i.e., that the angular distribution should be nearly constant in the measured back-angle angular region. The curves displayed in Fig. 2 correspond to χ^2/N values of 1.08, 0.62, 0.09, 0.09, 0.48, and 1.26 for $E_{c.m.}$ = 9.1, 9.9, 11.0, 11.7, 11.9, and 12.7 MeV, respectively. N stands for the number of degrees of freedom, i.e., the number of points minus one. Integration of such best-fit curves over the whole solid angle yields the experimental values of the total proton cross sections σ_p. Equivalently, σ_p can be obtained from the optimum σ_{fus} value by multiplying it by the respective proton multiplicity (M_p) also calculated by PACE2, i.e., $\sigma_p = M_p \times \sigma_{fus}$. These two procedures have been checked and give consistent results. The values of σ_p obtained are given in column 2 of Table II along with respective statistical uncertainties. It is worth mentioning that the uncertainties resulting from counting statistics were larger than those associated with the determination of the optimum fitting curves in Fig. 2, so the former uncertainties were used.

The possibility of having appreciable cross sections for the one-neutron transfer reaction ^{58}Ni(^{6}Li,^{5}Li)^{59}Ni is of some concern, because the ^{5}Li ejectile immediately decays ($T_{1/2} \sim 10^{-21}$ s) to $\alpha + p$, thus producing one proton for each transfer reaction ($M_p = 1$). Cross sections for this process (σ_{ntr}) were estimated by carrying out one-step Distorted Wave Born Approximation (DWBA) calculations with the code FRESCO [24]. A neutron-transfer spectroscopic factor Sn = 1.12 [25,26]

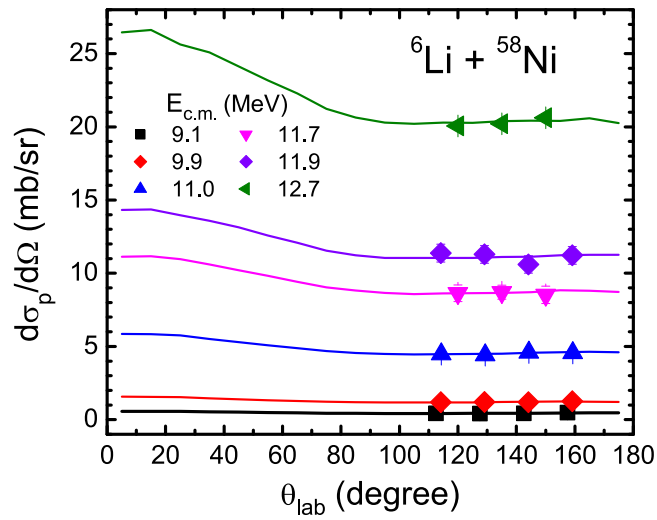

FIG. 2. Proton angular distribution obtained with the backward telescopes for each bombarding energy. The curves correspond to PACE2 calculations fitting the data.

TABLE II. Experimental (σ_p) and corrected ($\sigma_p^{\rm corr}$) proton cross sections for the ^{6}Li + ^{58}Ni system, respective proton multiplicities (M_p) obtained with three different codes, adopted $\langle M_p \rangle$ values, and the corresponding "fusion" cross sections. The three codes assumed $a = A/9.16$ and optical model potential (OMP) parameters from Ref. [21] for n and p, and from Ref. [22] for α. Total reaction cross sections (σ_R) are also given [23] for comparison purposes. Note: Values of $E_{\rm c.m.}$ for σ_R are 8.9, 10.2, 11.0, 11.8, and 12.7 MeV, respectively.

$E_{\rm c.m.}$ (MeV)	σ_p (mb)	$\sigma_p^{\rm corr}$ (mb)	M_p PACE2	M_p LILITA	M_p CASCADE	$\langle M_p \rangle$ ADOPTED	"$\sigma_{\rm fus}$" (mb)	σ_R (see Note)
9.1 ± 0.2	6.3 ± 0.4	4.0 ± 0.5	1.38	1.30	1.34	1.34 ± 0.06	3.0 ± 0.5	4 ± 2.7
9.9 ± 0.3	16.0 ± 0.7	9.8 ± 1.1	1.40	1.30	1.33	1.34 ± 0.06	7.3 ± 0.9	16.3 ± 9
11.0 ± 0.3	60.0 ± 3.9	41.8 ± 5.0	1.41	1.32	1.32	1.35 ± 0.05	31.0 ± 3.9	43.3 ± 12
11.7 ± 0.2	115.3 ± 8.4	84 ± 10	1.40	1.29	1.30	1.33 ± 0.06	63.2 ± 8.3	
11.9 ± 0.3	149 ± 11	110 ± 14	1.39	1.25	1.29	1.31 ± 0.07	84 ± 11	108 ± 36
12.7 ± 0.3	271 ± 3	218 ± 22	1.37	1.25	1.28	1.30 ± 0.07	168 ± 19	235 ± 52

was used for $^6\text{Li} \rightarrow {}^5\text{Li} + n$. This corresponds to assuming identical contributions from the $1/2^-$ and the $3/2^-$ angular momenta of the neutron and taking the respective quadratic sum. The neutron spectroscopic factors for $^{59}\text{Ni}^* \rightarrow {}^{58}\text{Ni} + n$ were taken from Ref. [27], where they were calculated by analyzing the (p,d) and (d,p) reactions on Ni isotopes via the adiabatic distorted wave approximation. We took into account neutron transfer reactions to the ground state (g.s.) and to 28 excited states of ^{59}Ni with excitation energies E^* up to 7.35 MeV, which correspond to the bound neutron states of ^{59}Ni. This interval of excitation energies includes the so-called Q window [28], where transfer reactions have the maximum yield. The value used for Sn (1.12), adopted because it was calculated from comparison with actual experimental data, is larger than the value obtained (∼0.68) from existing shell-model calculations [26,29]. The fact that the excitation spectrum of ^{59}Ni (more than 50 discrete states in this region) is only partially accounted for could possibly compensate for any overestimation of the neutron transfer cross section due to using an enlarged value of Sn. In any case, an overestimation of the neutron transfer cross section would lead to a respective underestimation of the corresponding fusion cross section, which would be safely absorbed in the systematic uncertainty that is assigned later in Sec. III.

Optical model potentials (OMPs) were used which describe well the $^6\text{Li} + {}^{58}\text{Ni}$ elastic scattering angular distributions reported in Ref. [23]. The same OMP also were used for the exit channel $^5\text{Li} + {}^{59}\text{Ni}$. The real and imaginary potential depths and the real diffuseness were fixed ($V_0 = 150$ MeV, $W_0 = 20$ MeV, $a_0 = 0.57$ fm), but a smooth energy dependence was used for the remaining geometrical parameters ($r_0 = 1.13$–1.25 fm, $r_W = 1.00$–1.12 fm, $a_W = 0.40$–0.74 fm). The Coulomb radius was $r_C = 1.2$ fm. Nuclear radii were calculated through the formula $R = r_0(A_1^{1/3} + A_2^{1/3})$. The potential binding the transferred neutron to the core was chosen to have a Woods-Saxon shape with fixed radius and diffuseness parameters, $r_0 = 1.25$ fm and $a_0 = 0.65$ fm. The depth of the central potential was adjusted to reproduce the experimental separation energies.

The estimated neutron transfer cross sections for the six energies in Table II, in increasing order, were $\sigma_{\rm ntr}$(mb) = 2.35, 6.25, 18.2, 31.2, 38.7, and 53.2, respectively. A 10% uncertainty was assigned to these values to account for sensitivity to the respective optical potential parameters. Because many excited states are populated, the overall angular distribution for ^{5}Li is rather smooth. Assuming that the respective decay protons are emitted isotropically (with multiplicity equal to one), the respective contribution to the experimental proton yield σ_p can be estimated for each bombarding energy. By subtracting this contribution, corresponding corrected proton cross sections $\sigma_p^{\rm corr}$ are obtained as listed in column 3 of Table II.

Strictly speaking, the measured proton yields also could include contributions from any process producing nuclei excited to energies above the respective proton emission threshold. In the case of the neutron transfer reaction discussed above, the value of $\sigma_{\rm ntr}$ peaks at an excitation energy of the ^{59}Ni residue of $E^* \sim 4.5$ MeV and it becomes negligible for $E^* > 7.3$ MeV. Because these energies are below the proton emission threshold for ^{59}Ni (8.60 MeV), no protons emitted by the ^{59}Ni residues are expected.

As for the one-proton transfer reaction $^{58}\text{Ni}(^6\text{Li},{}^5\text{He})^{59}\text{Cu}$, in this case the ejectile ^{5}He produces no protons because it decays to $\alpha + n$. The corresponding excitation energy of ^{59}Cu can be estimated, following Ref. [11], as $E^* = Q_{\rm gg} - Q_{\rm opt}$, where $Q_{\rm gg}$ is the ground-state Q value and the preferred Q value is $Q_{\rm opt} = (Z_3Z_4/Z_1Z_2 - 1)E_{\rm c.m.}$. In this expression, the entrance (exit) channels are denoted by subscripts 1 and 2 (3 and 4), respectively, and $E_{\rm c.m.}$ is the energy in the center-of-mass reference frame of the entrance channel. The estimated excitation energies for ^{59}Cu, for the energy range in the present experiment (see Table II), lie between 1.8 and 2.9 MeV, while the respective proton emission threshold is 3.42 MeV. Because the excitation energy is in principle distributed among all nucleons and in addition the proton inside the nucleus feels a Coulomb barrier, an excitation energy much above this threshold is needed for the proton to be emitted. Indeed, statistical model calculations performed with PACE2 indicate that in ^{59}Cu the proton-evaporation channel opens up at excitation energies above 8 MeV. Therefore, no contaminant protons are expected from the one-proton transfer reaction. The respective contribution, if any, was thus neglected. As for possible effects of direct reactions with the $\alpha + d$ or $^3\text{He} + t$ clusters in ^{6}Li, they are discussed later in Sec. III.

The respective M_p values calculated with PACE2 are given in column 4 of Table II. Possible model dependencies in M_p were

investigated following a procedure used earlier in connection with ^{8}B systems [30], by performing calculations with the two additional codes LILITA [31,32] and CASCADE (CASCIP version) [33,34]. Appropriate input parameters were chosen to assure that equivalent physical calculations were performed with the three codes. The mass table AME12 [35] and a level density parameter $a = A/9.16$ were always used. The latter expression fits existing data [36] in the mass region of interest ($54 \leqslant A \leqslant 64$). Columns 5 and 6 of Table II show the results obtained with the two additional codes, while column 7 gives the mean values of M_p for the three codes and the respective uncertainties. Finally, these mean values were used to deduce the fusion cross sections $\sigma_{\rm fus}$ displayed in column 8. The values of $\langle M_p \rangle \pm \delta\langle M_p \rangle$ should partially account for model-related effects, so the respective model dependencies are included in $\sigma_{\rm fus}$.

In the calculations of Table II, the OMP parameters were taken from Ref. [21] for neutrons and protons and from Ref. [22] for α particles. Additional model effects could arise from using different sets of OMP parameters. These effects were investigated by using in CASCADE the parameters recommended by the author of this code, i.e., from Becchetti and Greenlees [37] for protons, from Rapaport *et al.* [38] for neutrons, and from Satchler [39] for α particles. The corresponding values of M_p obtained for the energies listed in Table II, in increasing order, were 1.40, 1.40, 1.39, 1.37, 1.37, and 1.35, respectively. These numbers are consistent, within uncertainties, with the $\langle M_p \rangle$ values given in Table II. Therefore, no additional model dependency due to OMP parameters needs to be considered.

III. DISCUSSION OF RESULTS

Figure 3 shows the fusion cross sections of Table II, along with previous results [23] for total reaction cross sections

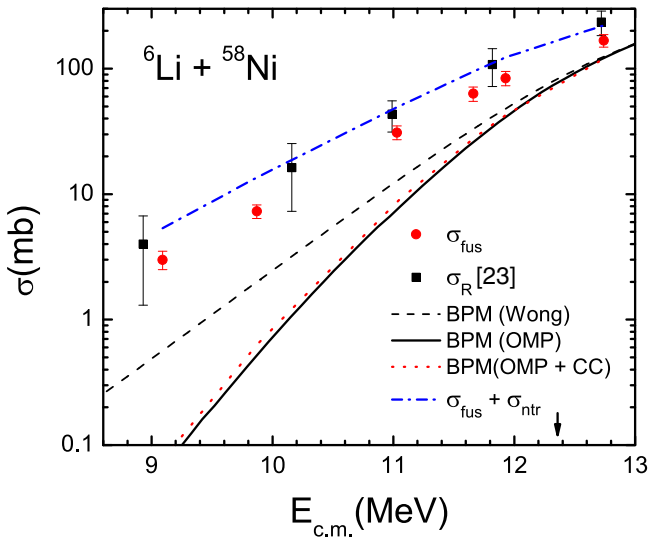

FIG. 3. Fusion excitation function obtained in the present work for the ^{6}Li + ^{58}Ni system. Also shown are the respective total reaction cross sections from Ref. [23], as well as results from BPM calculations and respective CC results, as described in the text. The dash-dotted line indicates that the sum $\sigma_{\rm fus} + \sigma_{\rm ntr}$, where $\sigma_{\rm ntr}$ represents a DWBA calculation for one-neutron transfer, nearly saturates σ_R.

for the same system. One-dimensional barrier penetration model (BPM) predictions using both Wong's formula [40] and the optical model are also shown. The respective barrier parameters, obtained by using the Sao Paulo potential (SPP) [41] for the bare nuclear potential, are $V_B = 12.36$ MeV, $R_B = 9.01$ fm, and $\hbar\omega_0 = 3.63$ MeV. A short-range Woods-Saxon imaginary potential ($W_0 = 50$ MeV, $r_W = 1.0$ fm, $a_W = 0.2$ fm) for the OMP calculation was added to the SPP to simulate an incoming wave boundary condition. The OMP result should be a more realistic BPM prediction due to the approximations involved in Wong's formula. The classical barrier height is indicated by the small vertical arrow in Fig. 3. Clearly, the experimental fusion cross sections show an enhancement with respect to these predictions, even for the one point measured above the barrier.

Possible effects of inelastic channels on fusion were investigated by assuming a vibrational model for ^{58}Ni. Inelastic excitations of the first 2^+ (1454 keV) and 3^- (4475 keV) states were included, with coupling strengths obtained from Refs. [42,43]. Only the ground state was considered for the ^{6}Li projectile, which has no bound excited states. As done above, fusion was identified with the absorption in the short-range imaginary potential. It is important to mention that this latter potential was not deformed by the couplings, consistent with the idea that inelastic scattering is a peripheral process. The results, obtained with the code FRESCO [24], are shown with the dotted line in Fig. 3. One concludes that the effect of inelastic couplings on fusion is insignificant if no other channels are included in the calculation. Therefore many more additional couplings would likely be required to get a good description of the data.

ICF, if present, cannot be distinguished from the present data, but it could alter the results. If the ^{6}Li projectile breaks into $\alpha + d$, for instance, ICF could occur with the ^{58}Ni target. ICF can be considered as a two-step process where first the projectile breaks into two clusters and then one of the clusters fuses with the target in a second step. For a given cluster x, its available energy $E^x_{\rm c.m.}$ after the first step, in the center-of-mass reference frame of the x-target system, can be estimated as [44]

$$E^x_{\rm c.m.} = \frac{m_x(m_p + m_t)}{m_p(m_x + m_t)}(E_{\rm c.m.} - S_x), \qquad (1)$$

where m denotes mass and subscripts x, p, and t refer to cluster, projectile, and target, respectively; $E_{\rm c.m.}$ corresponds to the p-t system; and S_x is the separation energy of cluster x in the projectile.

Statistical model calculations indicate that both ICF processes (with α or d) have a lower proton multiplicity than the CF process, i.e., where the whole ^{6}Li projectile fuses with ^{58}Ni. Depending on the particular ICF contribution, this means that part of the proton cross section ($\sigma_p^{\rm corr}$ in Table II) should be mapped into $\sigma_{\rm fus}$ by using an M_p value lower than the respective $\langle M_p \rangle$ value shown in Table II. Consequently, the presence of ICF would systematically increase the $\sigma_{\rm fus}$ values shown in Fig. 3. However, these values should not increase much because the sum $\sigma_{\rm fus} + \sigma_{\rm ntr}$ is already close to saturating σ_R, as the dash-dotted line in Fig. 3 shows.

TABLE III. Estimated excitation energies for respective compound systems after d- and α-ICF or DCT and after t- and ^{3}He-DCT. Results are shown for the maximum and minimum projectile energies in the present experiment.

$E_{\text{c.m.}}$ (^{6}Li + ^{58}Ni) (MeV)	E^*(^{60}Cu) (d-ICF) (MeV)	E^*(^{60}Cu) (d-DCT) (MeV)	E^*(^{62}Zn) (α-ICF) (MeV)	E^*(^{62}Zn) (α-DCT) (MeV)	E^*(^{61}Cu) (t-DCT) (MeV)	E^*(^{61}Zn) (^{3}He-DCT) (MeV)
9.1	14.0	12.6	8.6	7.7	3.7	1.1
12.7	15.3	13.7	11.1	10.1	4.8	3.4

Assuming that a 20% increase in σ_{fus} is still allowed (i.e., still consistent with σ_R, within uncertainties), some simple but cumbersome statistical model calculations render the following results: ICF contributions to the TF cross section could amount to up to 45% for ICF with d but only to a maximum of 25% for ICF with α. This is because $M_p(\alpha + {}^{58}\text{Ni}) < M_p(d + {}^{58}\text{Ni})$ for all experimental energies, so ICF with α's produces bigger changes in σ_{fus}. The σ_{fus} values reported in Table II should thus be considered as upper bounds for CF and lower bounds for TF. They could be taken as total fusion cross sections if a +20% systematic error is included. The plus sign (not minus) assigned to this uncertainty indicates that the actual value of σ_{TF} could be within 20% above the reported values.

In addition to $\alpha + d$, there is evidence for considerable $^3\text{He} + t$ clustering in ^{6}Li [45–49]. In fact, model calculations [47] indicate that even in the pure $\alpha + d$ model there is considerable $^3\text{He} + t$ (and $^5\text{He} + p$) clustering. Some authors, however, have concluded that the $^3\text{He} + t$ clustering is, at most, weak [50,51]. In any case, no effect of ICF with ^{3}He or t is expected in the present data because the respective separation energy in ^{6}Li is very large ($S_t = S_{^3\text{He}} = 15.8$ MeV) and using this value in Eq. (1) would produce unphysical negative energies for the clusters.

It is important to point out that direct cluster transfer (DCT) of α, d, ^{3}He, or t could also lead to the same compound systems as ICF with such clusters. We discuss first the case of clusters α and d. The excitation energies of the respective compound systems, which can be estimated as described in the previous section for the case of proton transfer (see also Ref. [11]), are similar for both processes (ICF and DCT), as seen from Table III. Because proton multiplicities are usually quite steady with energy (see Table II, for instance), similar values of M_p are expected for both processes ICF and DCT. Therefore, the discussion about α- and d-ICF in the previous paragraphs applies also to DCT. In other words, we cannot discard the possibility that some of the measured protons could come from DCT processes involving α or d clusters. If so, the respective yields would be correctly included in the above cross-section estimations. There are some hints that the dominant mechanism for capture of weakly bound clusters is ICF rather than DCT [52–55], but this cannot be assessed from the present experimental results. This is the reason for the quotation marks in "σ_{fus}" of Table II; they mean that the reported cross sections may have a contribution from α- and/or d-DCT.

As for possible effects of DCT involving t and ^{3}He clusters, columns 6 and 7 of Table III show the estimated excitation energies of the respective heavy residues. Considering that the proton emission threshold is 4.8 MeV for ^{61}Cu and 5.3 MeV for ^{61}Zn, it seems safe to neglect a possible contribution of these processes to the measured proton yield. This conclusion also is supported by PACE2 predictions indicating that the proton-evaporation channel in ^{61}Cu (^{61}Zn) opens up at excitation anergies above 9.5 (7.5) MeV, respectively

Summarizing, the reported fusion cross sections might include contributions from d- and/or α-ICF as well as from d- and/or α-DCT. On the other hand, no contribution from t- or ^{3}He-ICF or from p, t, or ^{3}He transfer is expected.

IV. COMPARISON WITH FUSION DATA FOR OTHER SYSTEMS WITH ^{6}Li PROJECTILES

We follow the prescription of Refs. [56–59] for the purpose of comparing fusion data for different systems. In this approach, the barrier parameters V_B, R_B, and $\hbar\omega_0$ are obtained from a realistic bare potential and used to reduce the cross section and the energy through the following expressions:

$$F(x) = \frac{2E}{\hbar\omega_0 {R_B}^2}\sigma_{\text{fus}}, \quad x = \frac{E - V_B}{\hbar\omega_0}. \tag{2}$$

The reduced cross sections can then be compared with the so-called universal fusion function (UFF) to find out whether the data present enhancement or suppression:

$$F_0(x) = \frac{2E}{\hbar\omega_0 {R_B}^2}\sigma^W = \ln[1 + e^{(2\pi x)}], \tag{3}$$

where σ^W stands for the expression derived for the cross section in the one-dimensional barrier-penetration model of Wong [40]. To avoid possible inaccuracies in Wong's model, such as those mentioned in connection with Fig. 3, the cross sections are renormalized with respect to the corresponding optical model (OM) calculations (solid curve in Fig. 3). The result is then multiplied by $F_0(x)$ (see Refs. [57–59]). In other words, instead of just using Eq. (2), the data are actually reduced according to the expression $(\sigma_{\text{fus}}/\sigma_{\text{OM}})F_0(x)$ or, equivalently,

$$\sigma_{\text{Red}}(x) = \frac{2E}{\hbar\omega_0 {R_B}^2}\sigma_{\text{fus}}\left(\frac{\sigma^W}{\sigma_{\text{OM}}}\right). \tag{4}$$

It is reasonable with this modified reduction to then compare the reduced data for different systems directly on the same plot, still using $F_0(x)$ as a standard reference even though Wong's model might fail for some data. We used always the double-folding SPP [41] to derive the barrier parameters, with default values for the matter and charge densities. These densities follow the systematics observed for many nuclei. Any deviations from the reference curve can then in principle be ascribed either to static effects, related to deviations in the

TABLE IV. Barrier parameters obtained from the São Paulo potential for the several relevant systems.

System	V_B (MeV)	R_B (fm)	$\hbar\omega_0$ (MeV)
^{6}Li + ^{59}Co	11.84	9.09	3.52
^{6}Li + ^{58}Ni	12.36	9.02	3.63
^{6}Li + ^{64}Ni	12.11	9.23	3.53
^{6}Li + ^{64}Zn	13.05	9.17	3.67

actual densities, or to dynamic effects, associated with some intrinsic properties of the nuclei involved.

In addition to the present data, fusion measurements with ^{6}Li projectiles have been performed for the similar-mass targets ^{59}Co [4], ^{64}Ni [60], and ^{64}Zn [11]. Table IV shows the barrier parameters used for each system, and the corresponding reduced results are presented in Fig. 4. One can observe from the figure for the lower-energy points corresponding to the ^{6}Li + ^{64}Zn system an apparent rise of the cross sections with decreasing energy. This has no physical meaning but reflects the fact that the ratio $\sigma^W/\sigma_{\rm OM}$ grows with decreasing energies faster than the corresponding cross sections decrease at these low energies.

Two features can be observed from Fig. 4: first, the data for the four targets follow similar trends, with considerable sub-barrier enhancement, and second, they actually show some spread in the considered energy region. The first observation could indicate that the mechanism responsible for the enhancement is mainly related to the ^{6}Li projectile, independent of the target. On the other hand, the reason underlying the second observation is probably related to effects of direct reactions such as those discussed in the previous two sections. In the case of the ^{6}Li + ^{64}Zn system, for instance, the authors of Ref. [11] mention that their data very probably include contributions from one-neutron and one-proton transfer reactions. This could

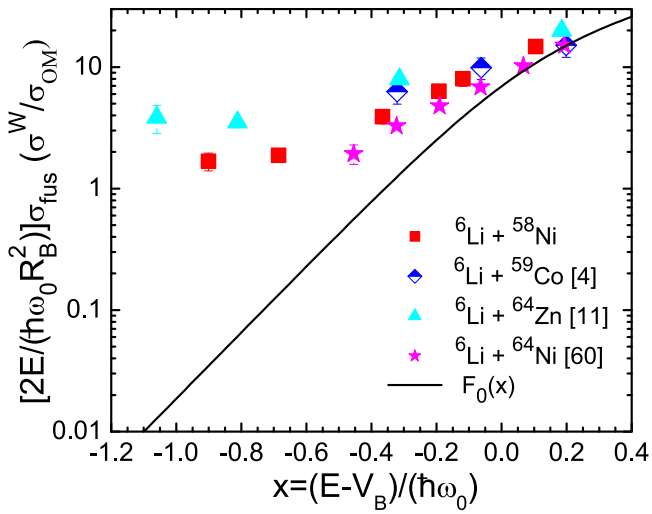

FIG. 4. Comparison of reduced fusion data for ^{6}Li projectiles with targets of ^{58}Ni (present work), ^{59}Co [4], ^{64}Ni [60], and ^{64}Zn [11]. Error bars are shown only if larger than symbol size. The curve corresponds to the UFF [Eq. (3)].

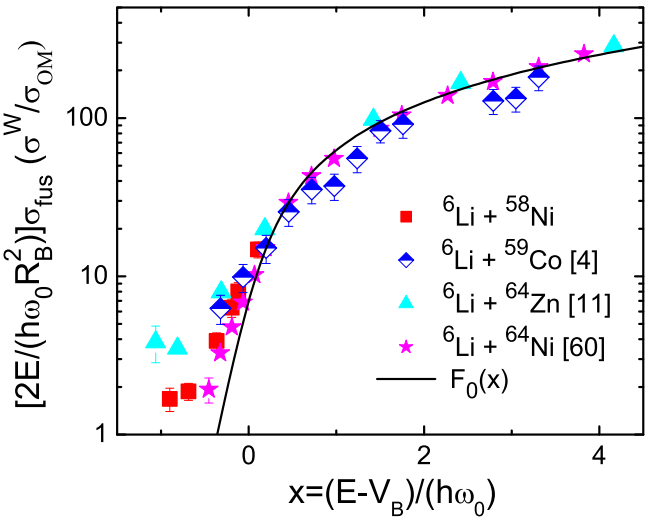

FIG. 5. Same as Fig. 4 but extended to include the full energy region where data have been measured.

explain the larger reduced cross sections as compared to the present data, which do not include such contributions. Similarly, the possible effects of different direct reactions, whose behavior is normally target dependent, could explain the spread of the data for the other systems in Fig. 4. Such effects could indeed be present in data taken with the γ-ray technique, because there is no way to distinguish whether the γ-emitting residue was created in a fusion-evaporation reaction or in a direct-transfer reaction.

It should be mentioned that the data sets for both ^{59}Co [4] and ^{64}Ni [60] were obtained using the γ-ray technique, while for the ^{64}Zn data the x-ray method was used [11]. The fairly good global agreement between all data sets indicates consistency between the three different experimental techniques involved. To pursue further this subject, the comparison made in Fig. 4 is extended in Fig. 5 to include all measured energies. If one takes into account that a 20% systematic uncertainty was reported for the data on ^{59}Co [4], it is valid to say that the three experimental techniques also are consistent with each other in the extended energy region.

V. CONCLUSIONS

Evaporation protons were measured for the ^{6}Li + ^{58}Ni reaction at six near- or sub-barrier energies and the relevant fusion cross sections were deduced. Corrections are made for effects of one-neutron transfer and arguments are given to show that contributions from p transfer as well as from reactions with the ^{3}He and t clusters can be neglected. In addition to ICF, the present results could include contributions from direct processes such as ^{2}H- or ^{4}He-DCT provided these reactions produce nuclei excited above the proton emission threshold. There are indications, though, that in this type of reaction the dominant mechanism is ICF rather than DCT. It is argued that the reported cross sections are actually upper (lower) bounds for CF (TF) and, by assigning an appropriate systematic uncertainty (+20%), they can be attributed to TF.

The data show a large sub-barrier enhancement with respect to expectations for a bare potential, with a lower but still sizable enhancement for the one point measured above the barrier. Corresponding CC calculations indicate that inelastic couplings by themselves have a negligible effect on fusion, and therefore many more additional channels would need to be considered to explain the data. From the experimental point of view, the need for obtaining a clean separation of the different reaction mechanisms in interactions of weakly bound projectiles with medium-mass targets in the near-barrier region has been previously emphasized [7]. From the theory point of view, continuum-continuum couplings using a realistic CDCC approach need to be investigated for the present system.

A comparison with data reported for ^{6}Li on targets of ^{59}Co, ^{64}Ni, and ^{64}Zn shows a fairly good global agreement between the respective reduced data, but some spread is observed especially at the lower energies. Differences at such energies between ^{58}Ni and ^{64}Zn data can probably be ascribed to nucleon-transfer contributions in the latter case. These types of contributions might also be present in the γ-ray data for ^{59}Co and ^{64}Ni. Therefore, target-dependent effects from direct processes might contribute to the enhancement at low energies producing the data spread observed. Nevertheless, we can conclude that a common mechanism probably related to the weakly bound structure of ^{6}Li is mainly responsible for the observed enhancement.

ACKNOWLEDGMENTS

E.F.A. acknowledges useful discussions with A. Di Pietro and is grateful for the warm hospitality of all personnel at Notre Dame during the measurements. This work has been partially supported by CONACYT (México) and by the NSF (USA) under Grants No. PHY14-01343 and No. PHY 14-01242. V.G. thanks the Conselho Nacional de Desenvolvimento Cientifico (CNPq) (Grant No. 302969/2013-6).

[1] B. B. Back, H. Esbensen, C. L. Jiang, and K. E. Rehm, Rev. Mod. Phys. **86**, 317 (2014).
[2] L. F. Canto, P. R. S. Gomes, R. Donangelo, J. Lubian, and M. S. Hussein, Phys. Rep. **596**, 1 (2015).
[3] J. J. Kolata, V. Guimarães, and E. F. Aguilera, Eur. Phys. J. A **52**, 123 (2016).
[4] C. Beck *et al.*, Phys. Rev. C **67**, 054602 (2003).
[5] A. Diaz-Torres, I. J. Thompson, and C. Beck, Phys. Rev. C **68**, 044607 (2003).
[6] C. Beck, N. Keeley, and A. Diaz-Torres, Phys. Rev. C **75**, 054605 (2007).
[7] C. Beck, N. Rowley, P. Papka, S. Courtin, M. Rousseau, F. A. Souza, N. Carlin, R. Liguori Neto, M. M. de Moura, M. G. Del Santo, A. A. P. Suaide, M. G. Munhoz, E. M. Szanto, A. Szanto de Toledo, N. Keeley, A. Diaz-Torres, and K. Hagino, Nucl. Phys. A **834**, 440c (2010).
[8] D. R. Otomar, P. R. S. Gomes, J. Lubian, L. F. Canto, and M. S. Hussein, Phys. Rev. C **87**, 014615 (2013).
[9] M. Zadro, P. Figuera, A. Di Pietro, M. Fisichella, M. Lattuada, T. Lönnroth, M. Milin, V. Ostashko, M. G. Pellegriti, V. Scuderi, D. Stanko, E. Strano, and D. Torresi, Phys. Rev. C **87**, 054606 (2013).
[10] J. P. Fernández-García, M. Zadro, A. Di Pietro, P. Figuera, M. Fisichella, O. Goryunov, M. Lattuada, C. Marchetta, A. M. Moro, A. Musumarra, V. Ostashko, M. G. Pellegriti, V. Scuderi, E. Strano, and D. Torresi, Phys. Rev. C **92**, 054602 (2015).
[11] A. Di Pietro, P. Figuera, E. Strano, M. Fisichella, O. Goryunov, M. Lattuada, C. Maiolino, C. Marchetta, M. Milin, A. Musumarra, V. Ostashko, M. G. Pellegriti, V. Privitera, G. Randisi, L. Romano, D. Santonocito, V. Scuderi, D. Torresi, and M. Zadro, Phys. Rev. C **87**, 064614 (2013).
[12] S. Kalkal, E. C. Simpson, D. H. Luong, K. J. Cook, M. Dasgupta, D. J. Hinde, I. P. Carter, D. Y. Jeung, G. Mohanto, C. S. Palshetkar, E. Prasad, D. C. Rafferty, C. Simenel, K. Vo-Phuoc, E. Williams, L. R. Gasques, P. R. S. Gomes, and R. Linares, Phys. Rev. C **93**, 044605 (2016).
[13] D. J. Hinde, M. Dasgupta, B. R. Fulton, C. R. Morton, R. J. Wooliscroft, A. C. Berriman, and K. Hagino, Phys. Rev. Lett. **89**, 272701 (2002).
[14] L. F. Canto, P. R. S. Gomes, R. Donangelo, and M. S. Hussein, Phys. Rep. **424**, 1 (2006).
[15] E. F. Aguilera, J. J. Kolata, E. Martinez-Quiroz, P. Amador-Valenzuela, D. Lizcano, A Gómez-Camacho, and A. García-Flores, J. Phys.: Conf. Ser. **639**, 012001 (2015).
[16] F. D. Becchetti and J. J. Kolata, Nucl. Instrum. Methods Phys. Res., Sect. B **376**, 397 (2016).
[17] E. F. Aguilera *et al.*, Phys. Rev. Lett. **107**, 092701 (2011).
[18] E. Martinez-Quiroz, E. F. Aguilera, D. Lizcano, P. Amador-Valenzuela, H. García-Martínez, J. J. Kolata, A. Roberts, L. O. Lamm, G. Rogachev, V Guimarães, F. D. Becchetti, A. Villano, M. Ojaruega, M. Febbraro, Y. Chen, H. Jiang, P. A. DeYoung, and G. F. Peaslee, Phys. Rev. C **90**, 014616 (2014).
[19] A. Gavron, Phys. Rev. C **21**, 230 (1980).
[20] A. Gavron, in *Computational Nuclear Physics 2. Nuclear Reactions*, edited by K. Langanke, J. A. Maruhn, and S. E. Koonin (Springer, New York, 1993), p. 108.
[21] C. M. Perey and F. G. Perey, At. Data Nucl. Data Tables **17**, 1 (1976).
[22] J. R. Huizenga and G. Igo, Nucl. Phys. **29**, 462 (1962).
[23] E. F. Aguilera, E. Martinez-Quiroz, D. Lizcano, A. Gómez-Camacho, J. J. Kolata, L. O. Lamm, V. Guimarães, R. Lichtenthäler, O. Camargo, F. D. Becchetti, H. Jiang, P. A. DeYoung, P. J. Mears, and T. L. Belyaeva, Phys. Rev. C **79**, 021601(R) (2009).
[24] I. J. Thompson, Comput. Phys. Rep. **7**, 167 (1988).
[25] L. A. Kull, Phys. Rev. **163**, 1066 (1967).
[26] J. Lee, M. B. Tsang, and W. G. Lynch, Phys. Rev. C **75**, 064320 (2007).
[27] J. Lee, M. B. Tsang, W. G. Lynch, M. Horoi, and S. C. Su, Phys. Rev. C **79**, 054611 (2009).
[28] G. R. Satchler, *Direct Nuclear Reactions* (Clarendon, Oxford, 1983).
[29] S. Cohen and D. Kurath, Nucl. Phys. A **101**, 1 (1967).
[30] E. F. Aguilera, P. Amador-Valenzuela, E. Martinez-Quiroz, J. Fernández-Arnáiz, J. J. Kolata, and V. Guimarães, Phys. Rev. C **93**, 034613 (2016).
[31] J. Gomez del Campo and R. G. Stokstad, ORNL Report TM-7295, 1981.

[32] J. Gomez del Campo (private communication).
[33] F. Pühlhofer, Nucl. Phys. A **280**, 267 (1977).
[34] M. N. Harakeh, D. H. Dowell, G. Feldman, E. F. Garman, R. Loveman, J. L. Osborne, and K. A. Snover, Phys. Lett. B **176**, 297 (1986).
[35] M. Wang, G. Audi, A. H. Wapstra, F. G. Kondev, M. MacCormick, X. Xu, and B. Pfeiffer, Chin. Phys. C **36**, 1603 (2012).
[36] R. G. Stokstad, in *Treatise on Heavy-Ion Science*, edited by D. A. Bromley (Plenum, New York, 1985), Vol. 3, p. 83.
[37] F. D. Becchetti, Jr. and G. W. Greenlees, Phys. Rev. **182**, 1190 (1969).
[38] J. Rapaport, V. Kulkarni, and R. W. Finlay, Nucl. Phys. A **330**, 15 (1979).
[39] G. R. Satchler, Nucl. Phys. **70**, 177 (1965).
[40] C. Y. Wong, Phys. Rev. Lett. **31**, 766 (1973).
[41] L. C. Chamon, B. V. Carlson, L. R. Gasques, D. Pereira, C. De Conti, M. A. G. Alvarez, M. S. Hussein, M. A. Cândido Ribeiro, E. S. Rossi, Jr., and C. P. Silva, Phys. Rev. C **66**, 014610 (2002).
[42] S. Raman, C. W. Nestor, Jr., and P. Tikkanen, At. Data Nucl. Data Tables **78**, 1 (2001).
[43] M. R. Bhat, Nucl. Data Sheets **80**, 789 (1997).
[44] E. F. Aguilera, E. Martinez-Quiroz, P. Rosales, J. J. Kolata, P. A. DeYoung, G. F. Peaslee, P. Mears, C. Guess, F. D. Becchetti, J. H. Lupton, and Y. Chen, Phys. Rev. C **80**, 044605 (2009).
[45] G. Bassani, N. Saunier, B. M. Traoré, G. Pappalardo, and A. Foti, J. Phys. Colloq. **32**, C6-133 (1971).
[46] M. F. Werby, M. B. Greenfield, K. W. Kemper, D. L. McShan, and S. Edwards, Phys. Rev. C **8**, 106 (1973).
[47] R. Beck, F. Dickmann, and R. G. Lovas, Ann. Phys. **173**, 1 (1987).
[48] R. G. Lovas, T. Kruppa, R. Beck, and F. Dickmann, Nucl. Phys. A **474**, 451 (1987).
[49] V. Zagrebaev, Heavy Ion Phys. **18**, 149 (2003).
[50] M. Rai, D. E. Lehman, and A. Ghovanlou, Phys. Lett. B **59**, 327 (1975).
[51] M. C. Etchegoyen, A. Etchegoyen, and E. Belmont Moreno, J. Phys. G: Nucl. Phys. **10**, 823 (1984).
[52] M. Dasgupta, P. R. S. Gomes, D. J. Hinde, S. B. Moraes, R. M. Anjos, A. C. Berriman, R. D. Butt, N. Carlin, J. Lubian, C. R. Morton, J. O. Newton, and A. Szanto de Toledo, Phys. Rev. C **70**, 024606 (2004).
[53] F. A. Souza, C. Beck, N. Carlin, N. Keeley, R. Liguori Neto, M. M. de Moura, M. G. Munhoz, M. G. Del Santo, A. A. P. Suaide, E. M. Szanto, and A. Szanto de Toledo, Nucl. Phys. A **821**, 36 (2009).
[54] F. A. Souza *et al.*, Eur. Phys. J. A **44**, 181 (2010).
[55] A. Shrivastava, A. Navin, A. Diaz-Torres, V. Nanal, K. Ramachandran, M. Rejmund, S. Bhattacharyya, A. Chatterjee, S. Kailas, A. Lemasson, R. Palit, V. V. Parkar, R. G. Pillay, P. C. Rout, and Y. Sawant, Phys. Lett. B **718**, 931 (2013).
[56] N. V. S. V. Prasad, A. M. Vinodkumar, A. K. Sinha, K. M. Varier, D. L. Sastry, N. Madhavan, P. Sugathan, D. O. Kataria, and J. J. Das, Nucl. Phys. A **603**, 176 (1996).
[57] L. R. Gasques, L. C. Chamon, D. Pereira, M. A. G. Alvarez, E. S. Rossi, Jr., C. P. Silva, and B. V. Carlson, Phys. Rev. C **69**, 034603 (2004).
[58] L. F. Canto, P. R. S. Gomes, J. Lubian, L. C. Chamon, and E. Crema, J. Phys. G: Nucl. Part. Phys. **36**, 015109 (2009).
[59] L. F. Canto, P. R. S. Gomes, J. Lubian, L. C. Chamon, and E. Crema, Nucl. Phys. A **821**, 51 (2009).
[60] Md. M. Shaikh, S. Roy, S. Rajbanshi, M. K. Pradhan, A. Mukherjee, P. Basu, S. Pal, V. Nanal, R. G. Pillay, and A. Shrivastava, Phys. Rev. C **90**, 024615 (2014).